



1 **On the Contribution of Fast and Slow Responses to**
2 **Precipitation Changes Caused by Aerosol Perturbations**

3 Shipeng Zhang¹, Philip Stier¹, Duncan Watson-Parris¹

4 ¹ Atmospheric, Oceanic and Planetary Physics, Department of Physics, University of Oxford, UK

5 *Correspondence to:* Shipeng Zhang (shipeng.zhang@physics.ox.ac.uk)

6

7

8 **Abstract.** Changes in global-mean precipitation are strongly constrained by global radiative cooling, while
9 regional rainfall changes are less constrained because energy can be transported. Absorbing and non-absorbing
10 aerosols have different effects on both global-mean and regional precipitation, due to the distinct effects on
11 energetics. This study analyses the precipitation responses to large perturbations in black carbon (BC) and
12 sulphate (SUL) respectively by examining the changes in atmospheric energy budget terms on global and
13 regional scales, in terms of fast (independent of changes in sea surface temperature (SST)) and slow responses
14 (mediated by changes in SST). Changes in atmospheric radiative cooling/heating are further decomposed into
15 contributions from clouds, aerosols, and clear-clean sky (without clouds or aerosols).

16 Both cases show a decrease in global-mean precipitation, dominated by fast responses in the BC case while slow
17 responses in the SUL case. The geographical patterns are distinct too. The intertropical convergence zone (ITCZ),
18 accompanied with tropical rainfall, shifts northward in the BC case, while southward in the SUL case. For both
19 cases, energy transport terms from the slow response dominates the changes in tropical rainfall, which are
20 associated with the northward (southward) shift of Hadley cell in response to the enhanced southward (northward)
21 cross-equatorial energy flux caused by increased BC (SUL) emission. The extra-tropical precipitation decreases
22 in both cases. For the BC case, fast responses to increased atmospheric radiative heating contribute most to the
23 reduced rainfall, in which absorbing aerosols directly heat the mid-troposphere, stabilise the column, and suppress
24 precipitation. Unlike BC, non-absorbing aerosols decrease surface temperatures through slow processes, cool the
25 whole atmospheric column, and reduce specific humidity, which leads to decreased radiative cooling from the
26 clean-clear sky, and is consistent with the reduced rainfall. Examining the changes in large-scale circulation and
27 local thermodynamics qualitatively explains the responses of precipitation to aerosol perturbations, whereas the
28 energetic perspective provides a method to quantify their contributions.

29



30 1. Introduction

31 Aerosols have been proposed to affect clouds and precipitation to a large extent by interacting with clouds and
32 radiation (Ramanathan et al., 2001). However, aerosol effects on clouds and precipitation remain highly uncertain
33 due to the complex nature of aerosol-cloud-radiation interactions. Knowledge about the chain of processes, from
34 aerosol emission to acting as cloud condensation nuclei (CCN) or ice nuclei (IN) and to cloud microphysics and
35 dynamics, is critical for reducing the uncertainties and understanding the climate system (Ghan et al., 2016),
36 which is referred to as a ‘bottom-up’ approach. However, this is challenging, considering uncertainties can arise
37 from aerosol emissions, activation, cloud microphysics and dynamic regimes (e.g., Gettelman et al., 2013; Ghan
38 et al., 2012; Michibata et al., 2016; Zhang et al., 2016).

39 An energetic perspective provides an alternative approach to examine aerosol effects on precipitation, which is
40 referred to as a ‘top-down’ approach. For global scales, in equilibrium, latent heat released from rainfall should
41 be energetically balanced by atmospheric radiative cooling together with surface energy fluxes (Allen and Ingram,
42 2002; Andrews et al., 2010). Climate forcers, such as greenhouse gases (GHGs) and aerosols, which affect the
43 energy budget, can modify the hydrological responses (Kvalevåg et al., 2013; Stephens and Hu, 2010). The energy
44 constraints can be applied to regional rainfall by introducing the energy transport term (H) (Muller and O’Gorman,
45 2011; Richardson et al., 2016). The local energy budget at equilibrium can be addressed as the following equation:

$$46 \quad L\delta P = \delta Q + \delta H \quad (1)$$

47 where δ denotes the difference between two climate states (e.g., with and without anthropogenic aerosols). L
48 refers to the latent heat of condensation, and P is the precipitation rate, so LP refers to the atmospheric latent
49 heating rate from rainfall. H is the column-integrated divergence of dry static energy which is expected to be zero
50 on a global scale. Q is the atmospheric diabatic cooling (except for latent heat released from precipitation),
51 consisting of atmospheric radiative cooling (ARC) and downward surface sensible heat flux (-SH). ARC is the
52 difference of shortwave (SW) and longwave (LW) fluxes between top of the atmosphere (TOA) and the surface.
53 ARC has significant impacts on global hydrological sensitivity (Allen and Ingram, 2002), while changes in the
54 energy transport term (δH) are essential in determining the spatial pattern of precipitation response (Muller and
55 O’Gorman, 2011). Dagan et al., (2019) further demonstrated that whether precipitation responses are more
56 correlated with changes in Q or H depends on the latitude considered. In the extra-tropics, diabatic cooling/heating
57 perturbations are confined to local scales due to strong Coriolis force (thus weak energy transport), and hence the
58 latent heating must balance diabatic cooling according to the energy budget. However, in the tropics, horizontal
59 gradients of dry static energy are small due to the weak Coriolis force and thus diabatic heating perturbations can
60 lead to thermally direct circulations which drive convergence/divergence of moisture and dry static energy. These
61 circulations cause low-level convergence of mass and moisture which drive vertical motion and thus an increase
62 in precipitation, so rainfall does not necessarily have to positively correlate with diabatic cooling (Dagan et al.,
63 2019).

64 Absorbing and non-absorbing aerosols can have different effects on each energy budget term, and thus
65 precipitation. On the global scale, black carbon (BC), a strongly absorbing aerosol, can stabilise the atmosphere
66 and suppress precipitation via strong shortwave absorption for short timescales, but also can increase precipitation
67 by warming up the surface temperature on longer timescales (e.g., Pendergrass and Hartmann, 2012). The net
68 effect can be uncertain among GCMs (Samset et al., 2016), and is sensitive to the altitude where the BC are added
69 (Ming et al., 2010). Unlike BC, non-absorbing aerosols, for example sulphate (SUL), reduce precipitation



70 predominantly by decreasing SST on long timescales through the dimming effect, whereby SUL scatters incoming
71 solar radiation back to the space (Boucher et al., 2013). Additionally, the surface sensible heat flux is more
72 sensitive to changes in BC than SUL (Myhre et al., 2018; Richardson et al., 2018). On zonal scales, due to the
73 relatively short lifecycle of aerosols, the radiative forcing caused by aerosols is hemispherically asymmetric,
74 which leads to a warmer northern hemisphere for the BC case and colder one for the SUL case, respectively. As
75 a result, the cross-equatorial energy fluxes lead to the intertropical convergent zone (ITCZ) shifting towards the
76 warmer hemisphere (Wang, 2009; Bischoff and Schneider, 2016; Zhao and Suzuki, 2019). On regional scales, it
77 is also worth noting that SUL is usually more likely to act as CCN due to the higher hygroscopicity compared to
78 BC. It can therefore alter regional rainfall by interacting with clouds, but the sign of changes in precipitation still
79 lacks agreement both in model simulations and observations (Bai et al., 2018; Haynes et al., 2009; Lebo and
80 Feingold, 2014).

81 These responses of precipitation have been conventionally suggested to be composed of fast and slow responses
82 (Andrews et al., 2009; Bala et al., 2010). Fast responses, on the timescale from days to months, are independent
83 of changes in sea surface temperature (SST), and mostly dependent on instantaneous changes in atmospheric
84 radiative heating/cooling (O’Gorman et al., 2012; Richardson et al., 2016). It should be noted that even though
85 SST is unchanged, the land surface temperature is generally still allowed to vary (Stjern et al., 2017). Slow
86 responses, on the timescale of years, are mediated by changes in sea surface temperature (SST) and strongly
87 correlate with top-of-atmosphere (TOA) forcing (Kvalevåg et al., 2013; Lambert and Webb, 2008; Suzuki et al.,
88 2017). Fast and slow responses are essential in determining changes in precipitation on both global and regional
89 scales. For example, Bony et al., (2013) examined the responses of tropical rainfall to increasing GHGs. They
90 found that the fast processes weaken the vertical motion and counteract a considerable part of the increasing trend
91 induced by surface warming. Shaw and Voigt (2015) have investigated predicted changes in the summertime
92 Asian monsoon under a warming scenario caused by GHGs, and the fast responses caused by direct radiative
93 effect are generally opposite to the slow impacts caused by the SST warming. The changes in circulation are
94 essential for local climate responses, including clouds, radiation and precipitation (Johnson et al., 2019), whereas
95 the spatial distribution of aerosols radiative forcing in turn affects atmospheric circulations (Chemke and Dagan,
96 2018).

97 Distinguishing contributions from different energetic terms is also helpful for understanding physical processes
98 and model differences (DeAngelis et al., 2015). It has historically been used to distinguish contributions from
99 clouds and aerosols when studying aerosol radiative forcing (Forster et al., 2007; Ghan 2013). While energetics
100 have been applied before to analyse precipitation responses (e.g., Ming et al., 2010; Dagan et al., 2019), here we
101 further decompose them into individual terms to provide additional insights. Changes in the energy transport term
102 (δH) can be decomposed into eddy and mean state components, which is further associated with changes in
103 thermodynamics and dynamics (Muller and O’Gorman, 2011; Richardson et al., 2016). Changes in ARC can be
104 further decomposed into contributions from aerosol (mostly through SW absorption), clouds (LW radiative
105 cooling), and clear-clean sky (mainly from water vapour, greenhouse gases, and the Plank feedback). While it has
106 long been appreciated that changes in ARC are essential in balancing latent heat release from precipitation
107 responses on global scales, their relationship on zonal mean or regional scales (and which ARC component
108 dominates) has not been fully explored.



109 The Precipitation Driver Response Model Intercomparison Project (PDRMIP) (Myhre et al., 2017) has conducted
110 several experiments to study the response of precipitation to different climate forcings, such as GHGs, aerosols,
111 and solar radiation change (e.g., Samset et al., 2016, Stjern et al., 2018). It has been found that the fast response
112 dominates the global-averaged precipitation responses to BC perturbation, which differs from other drivers of
113 climate change (Samset et al., 2017; Stjern et al., 2017). It has also been shown that BC contributes to the most
114 substantial uncertainties among GCMs in simulating the changes in surface temperature and precipitation, due to
115 different parameterisations of physical, chemical, and dynamical processes involved on the path from BC
116 emission to the final climate impact (e.g., Stjern et al., 2017). However, it is worth noting that most PDRMIP
117 research focuses on global mean changes and addressing uncertainties among GCMs (e.g., Myhre et al., 2017;
118 Richardson et al., 2018; Stjern et al., 2018). Samset et al., 2016 showed the spatial patterns of fast, slow and total
119 responses of precipitation to different climate forcings including absorbing and non-absorbing aerosols, with a
120 greater focus on the inter-comparison between different GCMs and different climate forcings. Here we study the
121 fast and slow response contribution to total response of precipitation with a focus on the comparison between
122 absorbing and non-absorbing aerosols, and in particular on the underlying mechanisms causing the differences by
123 distinguishing contributions from each energetic term at various scales.

124 In light of previous work illustrating the potential of energy budget constraints for understanding regional
125 precipitation changes, and the fact that absorbing and non-absorbing aerosols impact the response on two distinct
126 timescales, we aim to answer three questions: 1. What are the contributions of fast and slow responses to total
127 precipitation changes on global and regional scales? 2. What is the dominant energetic term in precipitation
128 responses to absorbing/non-absorbing aerosol perturbations on different scales? 3. How to relate changes in local
129 thermodynamics and large-scale circulation to changes in energetic terms and quantify their contribution to
130 precipitation responses?

131 2. Method

132 The global aerosol-climate model ECHAM6-HAM2 (Stier et al., 2005, Zhang et al., 2012, Tegen et al., 2019,
133 Neubauer et al., 2019) is used to perform all the experiments. It is based on the general circulation model
134 ECHAM6 (Stevens et al., 2013) and is coupled to the aerosol module HAM2 (Stier et al., 2005; Zhang et al.,
135 2012). A two-moment cloud microphysics schemes is used to prognostically predict the number and mass mixing
136 ratios for both cloud water and ice (Lohmann et al., 2007; Lohmann and Hoose, 2009). The parameterisations for
137 convection, including cumulus convection and deep convections, are based on the scheme by Tiedtke (1989) and
138 Nordeng (1994). The activation of CCN to cloud droplets is adopted from Abdul-Razzak and Ghan (2000), which
139 is based on Köhler theory (Köhler, 1936). The parameterisation for autoconversion is from Khairoutdinov and
140 Kogan (2000). There are 16 spectral shortwave bands in the solar radiation scheme, and 14 spectrum bands in the
141 longwave radiation scheme (Pincus and Stevens, 2013). The general circulation model ECHAM6 provides
142 essential meteorological backgrounds such as temperature, pressure, wind and humidity, which is coupled to
143 HAM2 for the parameterisations of several aerosol processes such as aerosol activation and deposition.

144 Emissions of anthropogenic BC, organic carbon and sulphate are from the Atmospheric Chemistry and Climate
145 Model Intercomparison Project (ACCMIP) emission dataset (Lamarque et al., 2010), including emissions from
146 industry, agriculture, aircraft, domestic, ships, and waste. Biomass burning emissions are also from ACCMIP
147 dataset, including both natural and anthropogenic biomass burning (Lamarque et al., 2010). Dimethyl sulphide



148 (DMS) emission is interactively related to the 10-meter wind speed and concentration in seawater. Biogenic
149 volatile organic carbon, and volcanic emissions are following the AeroCom phase II emission dataset (Dentener
150 et al., 2006). All the emissions are prescribed for the year 2000, so there are no interannual variabilities of
151 emissions. Simulations are performed at T63 ($1.9^\circ \times 1.9^\circ$) spectral resolution using 47 vertical levels (L47).

152 To study the precipitation response to absorbing and non-absorbing aerosol perturbations, we analyse two
153 scenarios: one with a ten-times increase in BC emissions and another with a five-times increase in sulphur dioxide,
154 relative to baseline emissions in the year 2000 (Tegen et al., 2019). As only particular aerosol emissions are
155 changed in each perturbation, the differences between baseline and the perturbed case can be interpreted as aerosol
156 effects. Geographical patterns of emission aerosol optical depth change can be found in the supplementary file
157 (Figure S1). This setup follows the PDRMIP experimental setup (Myhre et al., 2017).

158 We run the simulations for 100 years with a mixed layer ocean (MLO). To obtain the equilibrium state of
159 precipitation responses to aerosol perturbations, i.e. the total response (ΔP_{total}), we use the last 50 years of the
160 simulations because at that time the model has reached approximate equilibrium (Samset et al., 2016). Another
161 simulation is run for 20 years with fixed sea surface temperatures (fSST) and last ten years are used. The
162 precipitation responses for fSST simulations can be interpreted as the fast response (ΔP_{fast}). The slow response
163 is then calculated as the difference between the total response and the fast response (Myhre et al., 2017; Samset
164 et al., 2016):

$$165 \Delta P_{slow} = \Delta P_{total} - \Delta P_{fast} \quad (2)$$

166 The length of integration period is sufficient to derive the fast and total responses because the fast response of
167 precipitation occurs on time scales from days to months and a slower response on a time scale of years (Myhre et
168 al., 2017).

169 Since fast and slow responses are examined from an energetic perspective, we focus on how the atmospheric
170 diabatic cooling (Q) and energy transport terms (H) respond to aerosol perturbations in fSST and MLO
171 simulations. H is calculated as a residual by using the energy budget equation. Following previous studies (e.g.,
172 Muller and O’Gorman, 2011; Richardson et al., 2016), Q is the combination of atmospheric radiative cooling
173 (ARC) and downward surface sensible flux ($-SH$), as follows:

$$174 Q = ARC - SH \quad (3)$$

175 ARC is defined as net shortwave (SW) and longwave (LW) radiation loss of the atmospheric column, which can
176 be calculated from the difference between the top of atmosphere (TOA) and surface radiative fluxes (downward
177 positive), defined as

$$178 ARC = (LW_{TOA} + SW_{TOA}) - (LW_{SUR} + SW_{SUR}) \quad (4)$$

179 Ghan (2013) suggested using additional diagnostics to distinguish aerosol radiative forcing from aerosols, clouds,
180 and surface albedo. This has been widely adopted in current GCMs to better estimate aerosol effects (e.g., Zhang
181 et al., 2016). Following Ghan (2013), we further decompose ARC into contributions from clouds, aerosols and
182 clear-clean sky (without aerosols and clouds) separately (Equation 5), by using the same additional radiation call
183 to calculate ARC from the clear-clean sky ($ARC_{clear, clean}$):

$$184 ARC = ARC_{aerosol} + ARC_{cloud} + ARC_{clear, clean} \quad (5)$$

$$185 ARC_{aerosol} = ARC - ARC_{clear, clean} \quad (6)$$

$$186 ARC_{cloud} = ARC_{clear, clean} - ARC_{clear, clean} \quad (7)$$



187 Since ARC consists of radiative heating/cooling from aerosols (mainly through aerosol direct SW absorption),
188 clouds (primarily through cloud LW absorption/cooling), and clear-clean sky (mainly through LW radiative
189 absorption/cooling from GHGs, water vapour, and Planck feedback), it is helpful to systematically study the effect
190 of absorbing and non-absorbing aerosols on each decomposed energy term, and to further connect those to changes
191 in precipitation.

192 It is worth noting that $\Delta\text{ARC}_{\text{aerosol}}$ only includes direct interactions with radiation here and is much more sensitive
193 to absorbing aerosol burden rather than non-absorbing aerosols. Despite the significant negative radiative forcing
194 at TOA (Boucher et al., 2013), non-absorbing aerosols rarely modify atmospheric radiative absorption, as they
195 act to decrease net SW radiative fluxes at both the surface and TOA through scattering solar radiation. Non-
196 absorbing aerosols can affect atmospheric radiative absorption via changing absorbing aerosol life cycles (Stier
197 et al., 2006), but the impacts can be very small. It should also be noted here that changes in $\text{ARC}_{\text{cloud}}$ include
198 aerosol indirect effects (interactions with clouds) on ARC and cloud feedbacks in slow responses, but most of the
199 changes are from LW radiation from clouds (e.g., Lubin and Vogelmann, 2006) rather than SW radiation. And its
200 magnitude depends on the temperature (height) at both cloud top and bottom high as well as ice concentration at
201 cloud top (see Figure S2 for baseline $\text{ARC}_{\text{cloud}}$). As aerosol effects on convective clouds are not explicitly
202 simulated in ECHAM6-HAM2 (or most GCMs) yet, changes of $\text{ARC}_{\text{cloud}}$ from convective clouds are mostly
203 caused by aerosol-induced changes in dynamics. Baseline $\Delta\text{ARC}_{\text{aerosol}}$, $\Delta\text{ARC}_{\text{cloud}}$, and $\Delta\text{ARC}_{\text{clear, clean}}$ can be
204 seen in supplementary file (Figure S2, S3, S4).

205 3. Results

206 3.1. Global mean responses

207 Table 1 shows the global-mean fast, slow, and total responses of the energy budget terms, including atmospheric
208 latent heat release from precipitation ($L\Delta P$) and other atmospheric diabatic cooling terms, in response to increased
209 BC and SUL emission for the fSST and MLO simulations, respectively. Globally averaged precipitation is
210 decreased in both the BC and SUL experiment, and the associated reduced latent heating is primarily balanced by
211 decreased ARC (Table 1). However, there are some substantial differences between BC and SUL cases after
212 decomposition into different contributions.

213 For the BC case, the decreased precipitation from total responses ($L\Delta P$ around -3.26 W m^{-2}) is mostly contributed
214 by fast responses ($L\Delta P$ around -3.64 W m^{-2}). Slow responses ($L\Delta P$ around 0.38 W m^{-2}) lead to increased but much
215 smaller in magnitude precipitation changes compared to the fast responses. Previous studies suggest that fast
216 responses are largely mediated by atmospheric radiative absorption while slow responses scale with surface
217 temperature change (Samset et al., 2016). An increase of BC emissions can increase atmospheric absorption to a
218 large extent, which is a near-instantaneous process. This can be seen from the decomposition of ARC, which
219 shows that the decreased ARC from fast and total responses is mainly due to the increased SW absorption from
220 BC aerosols ($\Delta\text{ARC}_{\text{aerosol}}$) (Table 1). However, the change of global-mean surface temperature in the BC case is
221 small (around 0.4 K). That is because for an increase of BC emissions, reduction of downward SW radiation
222 largely counteracts increased downward LW radiation from the warmer atmosphere. As a result, the change of
223 surface temperature is regionally-dependent and globally small (Stjern et al., 2017) (Figure S2). Large changes in



224 $\Delta\text{ARC}_{\text{aerosol}}$ and small changes in global-mean surface temperature lead to a dominating contribution from fast
225 responses to total global-mean rainfall changes for the BC cases.
226 For the SUL case, the slow response dominates the total response (Table 1). Since SUL is a non-absorbing aerosol,
227 which decreases net SW radiative fluxes at both the surface and TOA through scattering solar radiation,
228 atmospheric absorption changes little. Most of the reduced ARC in the total response is from changes in clear-
229 clean sky radiative cooling ($\Delta\text{ARC}_{\text{cc}}$) from slow responses mediated via surface flux changes. As SUL decreases
230 SW radiation reaching the surface, the global-mean temperature decreases around 2K within a relatively long
231 timescale due to the high capacity of oceans (a slow process). Decreased global-mean temperature further leads
232 to reduced ARC_{cc} from decreased atmospheric column temperature (i.e. Planck feedback) (Zelinka et al., 2020),
233 and decreased water vapour content, which is controlled by the Clausius-Clapyron relationship (Suzuki and
234 Takemura, 2019).
235 The contribution of changes from SH acts to counteract nearly one-third the decreased ARC in fast and total
236 responses for the BC case, which is much larger than that in the SUL case. This is because the absorbing aerosols
237 heat the atmosphere and decrease the temperature difference between near-surface air and the surface, resulting
238 in reduced upward SH fluxes. So changes in SH are also dominated by the fast response, and mainly act to increase
239 precipitation from an energetic perspective, counteracting the decreasing effect induced by ARC in the BC case
240 (Ming et al., 2010).

241 3.2. Regional responses and their contributions

242 The geographical patterns of precipitation responses are substantially different between BC and SUL, in both the
243 fast and total responses (Figure 1). The patterns are similar to Samset et al., 2016, in which they showed an
244 ensemble result with a focus on inter-comparison among several models and climate forcings. For the total response,
245 it shows a distinct pattern of an ITCZ shift in response to increased BC and SUL emission. ITCZ tends to shift
246 northward in the BC case while southward in SUL case (Figure 1a and 1b). Since BC warms (SUL cools) the
247 northern hemisphere, there is an enhanced southward (northward) cross-equatorial energy flux in responses to the
248 aerosol perturbation, resulting in ITCZ being shifted towards the warmer hemisphere (Bischoff and Schneider,
249 2016; Wang, 2009). Changes in tropical rainfall are dominated by changes in the Hadley cell in responses to the
250 enhanced cross-hemispheric energy fluxes. Figure 1e and 1f further show that slow response mainly contributes
251 to the ITCZ shift in both cases. This will be further demonstrated in Section 3.3 and 3.4.
252 The fast response of precipitation in the BC case (Figure 1c) shows a land-sea contrast pattern in the tropics, in
253 which rainfall increases in central Africa while it decreases in the surrounding tropical ocean. Central Africa is
254 one of the main source regions of BC emission through biomass burning, and tenfold increase of BC emissions
255 makes the burden changes significant (Figure S1). The pattern of the fast precipitation response in the BC case is
256 similar to the pattern of rapid precipitation response to CO_2 shown in Richardson et al., (2016). But the mechanism
257 is not exactly the same. In the CO_2 case, even though SST remains unchanged, CO_2 can increase land surface
258 temperature and the land-sea temperature contrast (warmer land and unchanged ocean) leads to a shift of
259 convection to over land (Richardson et al., 2016). For an increase of BC emissions, increased downward LW
260 radiation from the warmer atmosphere is largely counteracted by a reduction of downward SW radiation. As a
261 result, surface temperature is decreased in central Africa (Figure S2), which differs from the CO_2 case. But
262 increased BC emission can still warm up the lower troposphere and lead to more ascending motions over Central



263 Africa (Figure S3) (Dagan et al., 2019; Roeckner et al., 2006). As for the SUL case, the rapid precipitation
264 response shows an opposite land-sea contrast pattern in the tropics, because SUL cools the land temperature
265 (Figure 1d) as land surface temperature is not constrained in fSST runs. However, considering SUL does not
266 directly affect the diabatic heating/cooling in the atmosphere, which differs from BC, the changes are small and
267 not statistically significant over most regions. There are still some exceptions. For example, southeast Asia, which
268 has the largest contribution to SUL emission, and SUL impacts on rainfall through cooling of land temperature as
269 well as interactions with monsoon (e.g., Wang et al., 2019). Decreased surface temperature over continents, such
270 as South America, leads to a decrease of precipitation in most land regions as well as an increase in surrounding
271 oceans (i.e. southeast Pacific Ocean). (Figure 1d).

272 In the zonal-mean, precipitation is decreased over northern hemispheric mid-latitudes in both BC and SUL cases
273 for total responses, but different processes contribute to the total response. Most of the precipitation changes over
274 high latitudes are contributed by fast responses in the BC case (Figure 1g) and slow responses in the SUL case
275 (Figure 1h). Dagan et al., (2019) showed different responses of rainfall to aerosol perturbation in the tropics and
276 extra-tropics. They demonstrated that precipitation responses are more correlated with the energy transport term
277 (H) in the tropics where heating anomalies can be compensated for by large-scale thermally-driven circulations,
278 whereas extra-tropical rainfall responses are constrained by radiative cooling in the extra-tropics due to the
279 stronger Coriolis force (thus weak energy transport). The different contribution from fast and slow processes
280 between the BC and SUL case indicates different responses in the diabatic cooling in the extra-tropics, and this
281 will be addressed in Figure 3 and Figure 4 from an energetic perspective.

282 Figure 2 quantifies how fast and slow responses contribute to total responses of precipitation on regional scales.
283 We used the response ratio which has also been used in Samset et al., (2016), as follows

$$284 R_{resp} = (|\Delta P_{fast}| - |\Delta P_{slow}|) / (|\Delta P_{fast}| + |\Delta P_{slow}|) \quad (8)$$

285 If R_{resp} is larger than 0 and close to 1, it means most of the total responses are contributed by fast responses. If
286 R_{resp} is less than 0 and close to -1, it means slow responses dominates over fast responses. Samset et al., (2016)
287 showed continental-based results of R_{resp} for different climate forcings, and found the variabilities among models.

288 Here Figure 2 focuses only on BC and SUL perturbations, and quantitatively gives us the geographical patterns
289 of contributions from fast and slow responses to total precipitation change. For the BC case, generally the response
290 over northern hemispheric midlatitudes is consistent with the globally averaged result shown in Table 1, in which
291 shows that the precipitation change is dominated by fast responses (Figure 2a). It can be seen from Figure 2a that
292 significant contribution from fast response over North America, northern Atlantic Ocean, Europe, most regions
293 in China, and north-eastern Pacifica Ocean. However, as for the changes in tropical rainfall, which is associated
294 with ITCZ shift seen in the total response, slow responses mainly contribute to the northward shift of ITCZ rather
295 than fast responses in the BC case. One exception is the Central Africa, where the precipitation changes are still
296 dominated by fast responses, and this will be further examined later. For the SUL case, it has been shown that
297 total responses are dominated by slow responses, both globally and regionally (Figure 2b). Some exceptions are
298 some land regions such as America, China and Sahel regions, where the precipitation change is mostly not
299 significant in total responses.



300 3.3. Changes in energy budget terms

301 To explain the different mechanisms between BC and SUL in terms of the contribution from fast and slow
302 responses in more detail, we examine the changes in each energy budget term from Equation 1.

303 For the BC case, in fast responses, most decreases in Q are located over the main BC source regions such as
304 Central Africa, Northeast China (Figure 3a and Figure S1). For zonal mean results, after decomposing δQ into
305 different terms based on Equation 3 and 5, it shows aerosol SW absorption is the major contributor to changes in
306 Q (Figure 5a). Since BC is a strongly absorbing aerosol, and the effect is near-instantaneous, the changes of Q
307 lead to decreased precipitation on global and zonal-mean scales and happen through fast responses (Table 1 and
308 Figure 5a). The zonal mean plot (Figure 3e) shows that fast responses of δQ caused by aerosol absorption (Figure
309 5a) leads to reduced rainfall, especially over northern hemispheric midlatitudes (red solid line in Figure 3e).

310 However, on regional scales, the energy transport term acts to play an important role. The geographical pattern of
311 precipitation changes (Figure 1c) is more similar to fast response of δH (Figure 3c) (spatial correlation ~ 0.9) than
312 δQ (spatial correlation ~ 0.5). The spatial pattern of fast δH (Figure 3c) also shows a land sea contrast in the
313 tropics as in the precipitation change distribution (Figure 1c), and this is most prominent in Central Africa and
314 middle Atlantic Ocean. There is a significant increase of rainfall over Central Africa and decrease over the middle
315 Atlantic Ocean (Figure 1a). This is mostly contributed by fast responses (Figure 1c and Figure 2a). As mentioned,
316 this pattern is similar to the case of CO_2 shown in Richardson et al., (2016). Although BC decreased surface
317 temperature in Central Africa through fast responses (Figure S2), BC can still warm up the lower troposphere at
318 central Africa, which results in a thermal driven circulation which favours more convections there. This is
319 evidenced by Figure 3c which shows the dry static energy flux flow from Central Africa to the middle Atlantic
320 Ocean (Figure 3c). Dagan et al., (2019) performed an idealised experiment by adding an absorbing plume in the
321 tropics, and found a very similar standing wave pattern of precipitation as a response. Examining δH shows that
322 this is caused by a thermal driven circulation, which favours more convections over central Africa. Positive δH is
323 consistent with more ascending motions at central Africa (Figure S3). BC warms up the lower troposphere at
324 central Africa, which results in more ascending motions (Figure S3), and the dry static energy flux flow from
325 Central Africa to the middle Atlantic Ocean (Figure 3c).

326 The slow response of δQ leads to a global increase of precipitation (Figure 3b), but the magnitude is an order of
327 magnitude less than the fast response in δQ . As precipitation responses in the extra-tropics are more correlated
328 with δQ , larger fast responses of Q explain why rainfall responses in extra-tropics are dominated by the fast
329 response in the BC case (Figure 2a). Figure 3e shows that the ITCZ shift seen in total responses is strongly
330 correlated with slow responses of δH . Warmer northern hemisphere caused by an increase in BC leads to a
331 southward cross-equatorial energy flux, which is accompanied by a northward shift of Hadley cell (Bischoff and
332 Schneider, 2016). Changes in vertical pressure velocity can be found in Figure 6, which also indicates a northward
333 shift of the ascending branch of the Hadley cell. From an energetic view, the changes in vertical pressure velocity
334 drive the dynamic effect on advection of dry static energy, which is a strong component in the changes of
335 divergence of dry static energy fluxes (δH) in the tropics (Richardson et al., 2016).

336 For the SUL case, most of the fast responses are not statistically significant (Figure 4a and 4c), and total responses
337 are dominated by the slow response. For changes in extra-tropics, changes in Q are correlated with changes in
338 precipitation. SUL decreases the mean-state temperature of troposphere through slow responses, which leads to a
339 reduction of specific humidity (Figure 7). From an energetic view, it leads to a decreased clean-clear sky radiative



340 cooling ($ARC_{clear, clean}$) (Figure 5d), which contributes to most of the reduced slow responses of δQ . For changes
341 in the tropics, like the BC case, slow responses of δH are consistent with the southward ITCZ shift in the total
342 response (Figure 4d). In the extra-tropics, there is also an interesting land-sea contrast in both fast and slow δH ,
343 with dry static energy fluxes generally diverging from oceans to lands in fast δH (Figure 4c) and converging in
344 slow δH (Figure 4d). This is because in the fixed SST simulations, land surface temperature is still allowed to
345 decrease in response to increased SUL emission (Figure S5b) as a result of reduced downward SW radiation. The
346 land-sea contrast of temperature (colder land) results in more downward large-scale motions and divergence of
347 moisture (See Figure S6 for changes in vertical pressure velocity and column-integrated water vapour) over most
348 land regions, particular Southeast Asia and South America, in fast responses. Since fast responses have already
349 accounted part of land temperature reduction, ocean surface temperature decreases more than land surface in slow
350 responses (Figure S2d). The colder ocean temperature therefore leads to a opposite land-sea pattern compared to
351 fast responses (Figure 4d).

352 Changes of Q are more robust in the fast response for the BC case, and the slow response of Q is more robust for
353 the SUL case. Decomposition of diabatic cooling shows its global-mean decrease is dominated by an increase of
354 atmospheric aerosol absorption for fast responses in BC case (Figure 5a) and decreased radiative cooling from the
355 clear-clean sky for slow responses in the SUL case (Figure 5d). The decreased $ARC_{clear, clean}$ are mainly caused
356 by the decreased atmospheric column temperature (Planck feedback) and associated reduced water vapour content
357 (controlled by the Clausius-Clapyron relationship). Sensible heat flux (upward) is also reduced due to the warmer
358 atmosphere caused by absorption from BC (Figure 5a).

359 It should also be noted that changes in diabatic cooling counteract the latent heat released from precipitation
360 associated with the ITCZ shift in both cases (Figure 3b and Figure 4b). This is mainly caused by ARC_{clouds} , as it
361 contributes a large part of diabatic cooling over tropical regions (Figure 5b and 5d). This counteraction with the
362 ITCZ shift is caused by the associated change of deep convective clouds (see supplementary file for changes in
363 cloud properties). This is consistent with the results shown in Naegele and Randall, (2019). They found a negative
364 correlation between tropical rainfall and diabatic cooling and demonstrated this is caused by feedbacks from deep
365 convective clouds. More high clouds lead to a decrease of atmospheric LW radiative cooling but an increase of
366 precipitation, and the negative correlation is robust over tropical regions where deep convective clouds prevail
367 (Naegele and Randall, 2019). The spatial patterns of fast, slow and total responses to $\Delta ARC_{aerosol}$, ΔARC_{cloud} ,
368 and $\Delta ARC_{clear, clean}$ can be found in supplementary file.

369 3.4. Responses of large-scale circulation and local thermodynamic conditions

370 Figure 3e and Figure 4e show that changes in tropical rainfall are strongly associated with slow responses of the
371 energy transport term, independent of aerosol types (absorbing or non-absorbing), whereas changes in mid-
372 latitude precipitation are dependent on aerosol types, which are dominated by fast responses of aerosol SW
373 absorption in the BC case and slow responses of clear-clean sky radiative cooling in the SUL case. To help
374 understand the mechanisms of the tropospheric response in different regions, we study the response of the large-
375 scale circulation and thermodynamic conditions, by examining the changes in vertical pressure velocity (ω),
376 temperature T , and specific humidity q (Figure 6 and Figure 7). The vertical pressure velocity (ω) at 500hPa is a
377 useful method to distinguish different cloud dynamic regimes, and a metric to quantify the strength of large-scale
378 circulation (Bony and Dufresne, 2005; Zhang et al., 2016). Here we only show zonal mean analysis.



379 As shown in Figure 6, BC warms up the atmosphere through SW absorption, and the warming is confined mainly
380 in the Northern Hemisphere (NH) where the BC emissions prevail. This leads to southward cross-equatorial
381 energy fluxes and northward shift of the Hadley cell (Wang, 2009; Bischoff and Schneider, 2016; Zhao and Suzuki,
382 2019). The changes in ω demonstrate the northward shift of the ascending branch of the Hadley cell, which show
383 an increased upward motion in NH tropics and decreased ascending motion in SH tropics (Figure 6d). Therefore,
384 the tropical rainfall associated with ITCZ changes in response to the changes of large circulation. Figure 6f further
385 demonstrates that slow responses contribute to most of the changes in tropical large-scale circulations in Figure
386 6d. It is consistent with Figure 3 that changes in tropical latent heat released from precipitation is mostly
387 contributed by $\delta H(\text{slow})$, because the dynamic component associated with changes vertical velocity dominates
388 the energy transport term over tropics (Richardson et al., 2016). Outside the tropics, changes in ω are not as
389 significant as in tropics (Figure 6d), and zonal mean rainfall is more related to local changes in thermodynamic
390 conditions. Absorbing aerosols directly heat the mid-troposphere through fast processes (Figure 6b). Heating the
391 mid-troposphere will stabilise the column and suppress precipitation. This is consistent with the energetic
392 perspective shown in Figure 3 and Figure 5a that fast responses of radiative cooling caused by BC SW absorption
393 (reduced $\text{ARC}_{\text{aerosol}}$) accounts for the decreased latent heat in extra-tropics. An interesting aspect here is that
394 while BC induces the ITCZ shift, the fast response (Figure 6e) seems to counteract the stronger slow response
395 shown in Figure 6f. This is because of the strong non-zonal effect from Central Africa (see geographical pattern
396 of vertical pressure velocity changes in the supplementary file), where BC warms up the lower troposphere
397 resulting in more ascending motions in fast responses (Figure S6). It is also consistent with Figure 1g that fast
398 responses of rainfall in southern tropical branch act to enhance ITCZ while only northern branch act to decrease
399 ITCZ.

400 For the SUL case, the tropical rainfall response is opposite to that in the BC case, but the mechanism is similar.
401 Increasing sulphate aerosols leads to reduced surface temperature due to the dimming effect of aerosols, and this
402 cooling is more significant in NH (Figure 7a). As a result, the northward cross-equatorial energy fluxes lead to a
403 southward shift of the Hadley cell (Figure 7d). The slow responses of the large-scale circulation (caused by SST
404 temperature difference between hemispheres) contributes most of the shift of Hadley cell (Figure 7e). In the extra-
405 tropics, a decrease of precipitation is also found in response to changes in thermodynamics. However, unlike black
406 carbon, SUL decreases surface temperature through slow processes and leads to a cooling of the whole column in
407 the extra-tropics (Figure 7a and 7c). As a result, the specific humidity shows a large reduction (Figure 7i), which
408 is associated with a reduction of rainfall in the extra-tropics. This is consistent with the energetic perspective
409 shown in Figure 4 and Figure 5d that reduced clean-clear sky radiative cooling ($\text{ARC}_{\text{clear, clean}}$) accounts for the
410 decreased latent heat in extra-tropics.

411 It is worth mentioning that Figure 6 and Figure 7, as a bottom-up method, qualitatively show how the changes in
412 large-scale circulation and local thermodynamics affect rainfall in terms of total, fast, and slow responses
413 respectively, whereas the energy budget view (Figure 3, 4, and 5), as a top-down method, is easier to quantify
414 these contributions through energetic terms (e.g., the energy transport term, $\text{ARC}_{\text{aerosol}}$ and $\text{ARC}_{\text{clear, clean}}$).
415 Combining these two methods makes the link between precipitation and aerosols explicit.



416 4. Conclusions

417 We have examined the response of precipitation to absorbing and non-absorbing aerosol perturbations by
418 separately increasing BC emission and SUL emission in ECHAM6-HAM2 by 10-times and 5-times their baseline
419 emission, following the PDRMIP protocol (Myhre et al., 2017; Samset et al., 2016). The precipitation response is
420 separated into fast (mediated by near-instantaneous changes in atmospheric radiative cooling) and slow responses
421 (mediated by changes in SST) on both global and regional scales. An energetic perspective has been adopted to
422 study precipitation changes. Global-averaged energetics have previously been used to study precipitation
423 responses (e.g., Ming et al., 2010; some PDRMIP work); here, we further decompose atmospheric heating rates
424 into individual terms separately for fast and slow responses. Changes in atmospheric latent heat release from
425 precipitation is balanced by changes in atmospheric radiative cooling (ARC), surface sensible heat flux and local
426 energy transport. We introduce a method, based on Ghan (2013), to further decompose ARC into contributions
427 from aerosols (through aerosol direct SW absorption), clouds (through cloud LW absorption/cooling), and clear-
428 clean sky (without aerosols or clouds; mainly through LW radiative absorption/cooling from GHGs, water vapour,
429 i.e. Planck feedback).

430 While it has long been appreciated that changes in ARC are essential in balancing latent heat released from
431 precipitation on global scales, their relationship on zonal mean or regional scales has not been fully explored. For
432 global means, although SUL and BC have a different sign of radiative forcing at TOA (Boucher et al., 2013), we
433 found that precipitation is decreased for both cases, which is energetically balanced by reduced atmospheric
434 diabatic cooling δQ (Table 1). This response occurs at different timescales, dominated by fast responses for BC
435 and by slow responses for SUL. For BC, on the global scale, the most significant effect is that absorbing aerosols
436 directly heat the mid-troposphere, stabilise the column, and suppress precipitation. Therefore, most of the changes
437 are due to aerosol absorption ($ARC_{aerosol}$) from fast responses. Meanwhile BC warms up the lower troposphere
438 and decrease the temperature differences between the surface and near-surface temperature, which results in a
439 decreased upward sensible heat. Investigating the energy balance, we found this decreased upward surface heat
440 fluxes from fSST experiment acts to cancel almost one third the decreasing effect caused by increased aerosol
441 SW absorption. For SUL, although non-absorbing aerosol does not directly affect ARC through aerosol absorption,
442 the net negative radiative forcing at TOA in fSST experiments and associated surface forcing leads to a decrease
443 of global surface temperature through slow responses. As a result, it cools the whole atmospheric column,
444 accompanied by reduced specific humidity, which leads to reduce precipitation. This can also be seen from the
445 decreased radiative cooling from the clean-clear sky $ARC_{clear, clean}$ in slow responses.

446 Zonally averaged patterns of precipitation changes for the BC and SUL cases are different (Figure 1). Tropical
447 rainfall is primarily associated with ITCZ, which shifts northward for BC, and southward for SUL. Extra-tropical
448 rainfall is reduced in both cases. For BC, slow responses account for most of the changes in tropical rainfall, while
449 fast responses dominate changes in other regions (Figure 2a). BC warms the northern hemisphere through slow
450 responses, which leads to a southward energy flux (Bischoff and Schneider, 2016; Rotstayn and Lohmann, 2002).
451 From an energetic perspective, in the tropics where intense convections and large-scale thermally driven
452 circulations prevail, slow responses of the energy transport term dominate the changes in tropical rainfall (Figure
453 3e), which is associated with the northward shift of Hadley cells (Figure 6). Outside the tropics, BC warms up the
454 mid-troposphere, stabilises the atmosphere (Figure 6) and suppresses precipitation, which is a fast response.
455 Energetically, different from the tropics, BC induced increased diabatic heating is locally confined due to stronger



456 Coriolis force. This geostrophic confinement of the diabatic heating associated with increased aerosols shortwave
457 absorption has to be balanced by reduced latent heat from precipitation (a fast response) (Figure 5a). For the SUL
458 case, the slow response dominates in nearly all regions (Figure 2b), which is not surprising given that sulphate
459 aerosol does not directly affect the column diabatic cooling. In the extra-tropics, SUL decreases surface
460 temperatures, primarily through slow processes, cools the whole column, and reduces specific humidity (Figure
461 7). From an energetic perspective, this can also be seen from the decreased radiative cooling from the clean-clear
462 sky (without clouds and aerosols) (Figure 5d) due to the reduced water vapour content and decreased atmospheric
463 column temperature (Planck feedback).

464 There exist some interesting regions where the responses are distinct from globally or zonally averaged results.
465 Rainfall is significantly increased over the Central Africa, in the BC case, together with reduced precipitation over
466 the middle Atlantic Ocean, and this pattern is most prominent in fast responses. This pattern shows clear
467 similarities with the standing wave pattern response of precipitation to an idealised plume of absorbing aerosols
468 in the tropics (Dagan et al., 2019). Examining δH shows that this is caused by a thermally driven circulation,
469 which favours more convections over central Africa. BC warms up the lower troposphere at central Africa, which
470 results in more ascending motions (Figure S3). The low latitude (thus weak Coriolis force) allows for the dry
471 static energy to be efficiently diverged from Central Africa to the middle Atlantic Ocean (Figure 3c). In the SUL
472 case, while most regions are dominated by slow responses, in some regions, such as most parts of China and South
473 America, rainfall changes are still dominated by fast responses (Figure 2b), where the surface temperature is
474 significantly decreased (Figure S2). This is due to the dimming effect from SUL and associated surface flux
475 changes, and because changes of land surface temperature are not constrained in fSST experiments. Reduced
476 surface fluxes and temperatures therefore lead to a decrease of precipitation over most land regions as well as an
477 increase at surrounding oceans (e.g., southeast Pacific Ocean).

478 Changes in zonally averaged vertical pressure velocity, temperature profile, and specific humidity (Figure 6 and
479 Figure 7) show consistency with zonally averaged energetics. Changes in vertical pressure velocity indicate a
480 northward shift of the ascending branch of the Hadley cell in the BC case and SUL case. It is consistent with the
481 changes in the divergence of dry static energy fluxes, which is dominated by the changes in vertical velocity (the
482 dynamic component) in the tropics (Richardson et al., 2016). In the extra-tropics, stabilisation induced by BC
483 through fast response is consistent with increased atmospheric radiative heating from aerosol SW absorption.
484 Reduced specific humidity as well as decreased atmospheric column temperature in the SUL case is consistent
485 with decreased radiative cooling from the clean-clear sky. The changes in large-scale circulations and local
486 thermodynamics qualitatively explains the responses of precipitation, whereas the energetic perspective provides
487 a method to quantify and make their contributions explicit.

488 In summary, we examined the relationship between aerosol-induced changes in atmospheric energetics and
489 precipitation changes across different scales. Generally, global-average and extra-tropical changes in ARC and
490 latent heat from precipitation are largely balanced and less balanced in the tropics due to efficient local energy
491 transport. We introduced a new decomposition method, derived from Ghan (2013), to examine aerosol effects on
492 precipitation. For absorbing aerosols, decreased global-mean and extra-tropical precipitation is associated with
493 increased atmospheric aerosol SW absorption from fast responses, while for non-absorbing aerosols, reduced
494 rainfall is more correlated with decreased clear-clean sky atmospheric radiative cooling from slow responses. This



495 top-down method, together with traditional bottom-up method, can make the link between precipitation and
496 aerosols explicit and quantify contributions to global and regional rainfall changes.
497 This metric provides further insights into the model variability in simulating rainfall and their responses to
498 different climate forcings, as shown by some PDRMIP research (e.g., Richardson et al., 2018; Stjern et al., 2018).
499 For example, it has been demonstrated that the response from BC perturbation contributes to a large part of the
500 substantial uncertainties among GCMs in simulating the changes in surface temperature and therefore
501 precipitation (Stjern et al., 2017). Distinguishing contributions from individual energetic terms is helpful to assess
502 uncertainties from aerosol absorption, or feedbacks from clouds, water vapour and surface sensible heat flux. This
503 will improve our understanding of GCMs and the climate system, which will be the focus of our follow-up work.
504 There exist some caveats when considering real-world implications of our results. The aerosol perturbation
505 follows the PDRMIP protocol designed to reveal the fundamental mechanisms and to make the aerosol effect
506 strong enough to be distinguishable from natural variability. However, these perturbations are too large to be
507 representative for real-world situations, in particular considering anthropogenic SO₂ (the precursor of SUL)
508 emissions that are starting to decrease in South-east Asia (Zheng et al., 2018). As for Northern Hemispheric
509 midlatitudes, where the population is concentrated, results here show that increased BC or SUL will lead to
510 decreased precipitation, but this happens at different time scales. Increased BC may lead to a near-instantaneous
511 decreased precipitation over China or America, while increased SUL will reduce precipitation via the slow
512 response, modulated by SSTs, at a much longer time scale. In the real world, it should be mentioned that the
513 anthropogenic emissions create a mixture of absorbing and non-absorbing aerosols, so the changes in rainfall
514 strongly depend on the time scale and the real-world emission scenario. It should also be noted that the total
515 responses of precipitation in this work are derived from mixed-layer ocean experiments and therefore differ from
516 real-world changes involving changes in the ocean circulation. There are several studies that have addressed the
517 importance of using ocean-coupled models to accurately simulate regional and global precipitation responses
518 (e.g., Wang et al., 2017; Zhao and Suzuki, 2019).

519
520 **Data availability:** The datasets of original simulations are from the ARCHER facility upon request. The data
521 used to present in this paper can be found at: <http://dx.doi.org/10.17632/8n2vj578r2.1> (Zhang, 2021)
522

523
524 **Author Contributions:** SZ carried out the simulations and analyses. DW and PS assisted with the simulations.
525 SZ prepared the paper with contributions from all co-authors.
526

527 **Acknowledgements:** The simulations were performed on the ARCHER UK National Supercomputing Service.
528 This research was supported by the European Research Council (ERC) project constRaining the EffeCts of
529 Aerosols on Precipitation (RECAP) under the European Union's Horizon 2020 research and innovation
530 programme with grant agreement no. 724602. DWP and PS also receive funding from the European Union's
531 Horizon 2020 research and innovation programme iMIRACLI under Marie Skłodowska-Curie grant agreement
532 No 860100. DWP also gratefully acknowledges funding from the NERC ACRUISE project NE/S005390/1.
533 Many thanks to Guy Dagan, Andrew Williams, Duo Chan, and Xianglin Dai for helpful discussions.
534



535

536 **References**

- 537 Abdul-Razzak, H. and Ghan, S. J.: A parameterization of aerosol activation: 2. Multiple aerosol types, *J. Geophys.*
538 *Res. Atmos.*, 105(D5), 6837–6844, doi:10.1029/1999JD901161, 2000.
- 539 Allen, M. R. and Ingram, W. J.: Constraints on future changes in climate and the hydrologic cycle, *Nature*,
540 419(6903), doi:10.1038/nature01092, 2002.
- 541 Andrews, T., Forster, P. M. and Gregory, J. M.: A surface energy perspective on climate change, *J. Clim.*, 22(10),
542 2557–2570, doi:10.1175/2008JCLI2759.1, 2009.
- 543 Andrews, T., Forster, P. M., Boucher, O., Bellouin, N. and Jones, A.: Precipitation, radiative forcing and global
544 temperature change, *Geophys. Res. Lett.*, 37(14), doi:10.1029/2010GL043991, 2010.
- 545 Bai, H., Gong, C., Wang, M., Zhang, Z. and L'Ecuyer, T.: Estimating precipitation susceptibility in warm marine
546 clouds using multi-sensor aerosol and cloud products from A-Train satellites, *Atmos. Chem. Phys.*, 18(3), 1763–
547 1783, doi:10.5194/acp-18-1763-2018, 2018.
- 548 Bala, G., Caldeira, K. and Nemani, R.: Fast versus slow response in climate change: Implications for the global
549 hydrological cycle, *Clim. Dyn.*, 35(2), 423–434, doi:10.1007/s00382-009-0583-y, 2010.
- 550 Bischoff, T. and Schneider, T.: The equatorial energy balance, ITCZ position, and double-ITCZ bifurcations, *J.*
551 *Clim.*, 29(8), 2997–3013, doi:10.1175/JCLI-D-15-0328.1, 2016.
- 552 Bony, S. and Dufresne, J. L.: Marine boundary layer clouds at the heart of tropical cloud feedback uncertainties
553 in climate models, *Geophys. Res. Lett.*, 32(20), 1–4, doi:10.1029/2005GL023851, 2005.
- 554 Bony, S., Bellon, G., Klocke, D., Sherwood, S. and Fermepin, S.: Robust direct effect of carbon dioxide on tropical
555 circulation and regional precipitation, *Nat. Geosci.*, 6(6), 447–451, doi:10.1038/ngeo1799, 2013.
- 556 Boucher, O., Randall, D., Artaxo, P., Bretherton, C., Feingold, G., Forster, P., Kerminen, V.-M. V.-M., Kondo,
557 Y., Liao, H., Lohmann, U., Rasch, P., Satheesh, S. K., Sherwood, S., Stevens, B., Zhang, X. Y. and Zhan, X. Y.:
558 Clouds and Aerosols, *Clim. Chang. 2013 Phys. Sci. Basis. Contrib. Work. Gr. I to Fifth Assess. Rep. Intergov.*
559 *Panel Clim. Chang.*, 571–657, doi:10.1017/CBO9781107415324.016, 2013.
- 560 Chemke, R. and Dagan, G.: The effects of the spatial distribution of direct anthropogenic aerosols radiative forcing
561 on atmospheric circulation, *J. Clim.*, 31(17), 7129–7145, doi:10.1175/JCLI-D-17-0694.1, 2018.
- 562 Dagan, G., Stier, P. and Watson-Parris, D.: Contrasting Response of Precipitation to Aerosol Perturbation in the
563 Tropics and Extratropics Explained by Energy Budget Considerations, *Geophys. Res. Lett.*, 46(13), 7828–7837,
564 doi:10.1029/2019GL083479, 2019.
- 565 DeAngelis, A. M., Qu, X., Zelinka, M. D. and Hall, A.: An observational radiative constraint on hydrologic cycle
566 intensification, *Nature*, 528(7581), 249–253, doi:10.1038/nature15770, 2015.



- 567 Dentener, F., Kinne, S., Bond, T., Boucher, O., Cofala, J., Generoso, S., Ginoux, P., Gong, S., Hoelzemann, J. J.,
568 Ito, A., Marelli, L., Penner, J. E., Putaud, J.-P., Textor, C., Schulz, M., van der Werf, G. R. and Wilson, J.:
569 Emissions of primary aerosol and precursor gases in the years 2000 and 1750 prescribed data-sets for AeroCom,
570 *Atmos. Chem. Phys.*, 6(12), 4321–4344, doi:10.5194/acp-6-4321-2006, 2006.
- 571 Forster, P., Ramaswamy, V., Artaxo, P., Bernsten, T., Betta, R., Fahey, D. W., Haywood, J., Lean, J., Lowe, D.
572 C., Myhre, G., Nganga, J., Prinn, R., Raga, G., Schulz, M., and Van Dorland, R.: Changes in atmospheric
573 constituents and in radiative forcing, in *Climate Change 2007: The Physical Science Basis. Contribution of*
574 *Working Group I to the Fourth Assessment Report of the Intergovernmental Panel on Climate Change*, edited by:
575 Solomon, S., Qin, D., Manning, M., Chen, Z., Marquis, M., Averyt, K. B., Tignor, M., and Miller, H. L.,
576 Cambridge University Press, New York, NY, 2007.
- 577 Gettelman, A., Morrison, H., Terai, C. R. and Wood, R.: Microphysical process rates and global aerosol-cloud
578 interactions, *Atmos. Chem. Phys.*, 13(19), 9855–9867, doi:10.5194/acp-13-9855-2013, 2013.
- 579 Ghan, S., Wang, M., Zhang, S., Ferrachat, S., Gettelman, A., Griesfeller, J., Kipling, Z., Lohmann, U., Morrison,
580 H., Neubauer, D., Partridge, D. G., Stier, P., Takemura, T., Wang, H. and Zhang, K.: Challenges in constraining
581 anthropogenic aerosol effects on cloud radiative forcing using present-day spatiotemporal variability, *Proc. Natl.*
582 *Acad. Sci.*, 113(21), 5804–5811, doi:10.1073/pnas.1514036113, 2016.
- 583 Ghan, S. J.: Technical Note: Estimating aerosol effects on cloud radiative forcing, *Atmos. Chem. Phys.*, 13(19),
584 9971–9974, doi:10.5194/acp-13-9971-2013, 2013.
- 585 Ghan, S. J., Liu, X., Easter, R. C., Zaveri, R., Rasch, P. J., Yoon, J. H. and Eaton, B.: Toward a minimal
586 representation of aerosols in climate models: Comparative decomposition of aerosol direct, semidirect, and
587 indirect radiative forcing, *J. Clim.*, 25(19), 6461–6476, doi:10.1175/JCLI-D-11-00650.1, 2012.
- 588 Haynes, J. M., L’Ecuyer, T. S., Stephens, G. L., Miller, S. D., Mitrescu, C., Wood, N. B. and Tanelli, S.: Rainfall
589 retrieval over the ocean with spaceborne W-band radar, *J. Geophys. Res. Atmos.*, 114(8), 1–18,
590 doi:10.1029/2008JD009973, 2009.
- 591 Johnson, B. T., Haywood, J. M. and Hawcroft, M. K.: Are Changes in Atmospheric Circulation Important for
592 Black Carbon Aerosol Impacts on Clouds, Precipitation, and Radiation?, *J. Geophys. Res. Atmos.*, 124(14), 7930–
593 7950, doi:10.1029/2019jd030568, 2019.
- 594 Khairoutdinov, M. and Kogan, Y.: A New Cloud Physics Parameterization in a Large-Eddy Simulation Model of
595 Marine Stratocumulus, *Mon. Weather Rev.*, 128(1), 229–243, doi:10.1175/1520-
596 0493(2000)128<0229:ANCPPI>2.0.CO;2, 2000.
- 597 Köhler, H.: The nucleus in and the growth of hygroscopic droplets, *Trans. Faraday Soc.*,
598 doi:10.1039/TF9363201152, 1936.
- 599 Kvalevåg, M. M., Samset, B. H. and Myhre, G.: Hydrological sensitivity to greenhouse gases and aerosols in a
600 global climate model, *Geophys. Res. Lett.*, 40(7), 1432–1438, doi:10.1002/grl.50318, 2013.



- 601 Lamarque, J.-F., Bond, T. C., Eyring, V., Granier, C., Heil, A., Klimont, Z., Lee, D., Liousse, C., Mieville, A.,
602 Owen, B., Schultz, M. G., Shindell, D., Smith, S. J., Stehfest, E., Van Aardenne, J., Cooper, O. R., Kainuma, M.,
603 Mahowald, N., McConnell, J. R., Naik, V., Riahi, K. and van Vuuren, D. P.: Historical (1850–2000) gridded
604 anthropogenic and biomass burning emissions of reactive gases and aerosols: methodology and application,
605 *Atmos. Chem. Phys.*, 10(15), 7017–7039, doi:10.5194/acp-10-7017-2010, 2010.
- 606 Lambert, F. H. and Webb, M. J.: Dependency of global mean precipitation on surface temperature, *Geophys. Res.*
607 *Letts.*, 35(16), 1–5, doi:10.1029/2008GL034838, 2008.
- 608 Lebo, Z. J. and Feingold, G.: On the relationship between responses in cloud water and precipitation to changes
609 in aerosol, *Atmos. Chem. Phys.*, 14(21), 11817–11831, doi:10.5194/acp-14-11817-2014, 2014.
- 610 Lohmann, U. and Hoose, C.: Sensitivity studies of different aerosol indirect effects in mixed-phase clouds, *Atmos.*
611 *Chem. Phys.*, 9(22), 8917–8934, doi:10.5194/acp-9-8917-2009, 2009.
- 612 Lohmann, U., Stier, P., Hoose, C., Ferrachat, S., Kloster, S., Roeckner, E. and Zhang, J.: Cloud microphysics and
613 aerosol indirect effects in the global climate model ECHAM5-HAM, *Atmos. Chem. Phys.*, 7(13), 3425–3446,
614 doi:10.5194/acp-7-3425-2007, 2007.
- 615 Lubin, D. and Vogelmann, A. M.: A climatologically significant aerosol longwave indirect effect in the Arctic,
616 *Nature*, 439(7075), 453–456, doi:10.1038/nature04449, 2006.
- 617 Michibata, T., Suzuki, K., Sato, Y. and Takemura, T.: The source of discrepancies in aerosol–cloud–precipitation
618 interactions between GCM and A-Train retrievals, *Atmos. Chem. Phys.*, 16(23), 15413–15424, doi:10.5194/acp-
619 16-15413-2016, 2016.
- 620 Ming, Y., Ramaswamy, V. and Persad, G.: Two opposing effects of absorbing aerosols on global-mean
621 precipitation, *Geophys. Res. Letts.*, 37(13), 1–4, doi:10.1029/2010GL042895, 2010.
- 622 Muller, C. J. and O’Gorman, P. A.: An energetic perspective on the regional response of precipitation to climate
623 change, *Nat. Clim. Chang.*, 1(5), 266–271, doi:10.1038/nclimate1169, 2011.
- 624 Myhre, G., Forster, P. M., Samsset, B. H., Odnebrog, Sillmann, J., Aalbergsjø, S. G., Andrews, T., Boucher, O.,
625 Faluvegi, G., Fläschner, D., Iversen, T., Kasoar, M., Kharin, V., Kirkevag, A., Lamarque, J. F., Olivie, D.,
626 Richardson, T. B., Shindell, D., Shine, K. P., Stjern, C. W., Takemura, T., Voulgarakis, A. and Zwiers, F.:
627 PDRMIP: A precipitation driver and response model intercomparison project-protocol and preliminary results,
628 *Bull. Am. Meteorol. Soc.*, 98(6), 1185–1198, doi:10.1175/BAMS-D-16-0019.1, 2017.
- 629 Naegele, A. C. and Randall, D. A.: Geographical and Seasonal Variability of Cloud-Radiative Feedbacks on
630 Precipitation, *J. Geophys. Res. Atmos.*, 124(2), 684–699, doi:10.1029/2018JD029186, 2019.
- 631 Neubauer, D., Ferrachat, S., Siegenthaler-Le Drian, C., Stier, P., Partridge, D. G., Tegen, I., Bey, I., Stanelle, T.,
632 Kokkola, H. and Lohmann, U.: The global aerosol–climate model ECHAM6.3–HAM2.3 – Part 2: Cloud
633 evaluation, aerosol radiative forcing, and climate sensitivity, *Geosci. Model Dev.*, 12(8), 3609–3639,
634 doi:10.5194/gmd-12-3609-2019, 2019.



- 635 Nordeng, T. E.: Extended versions of the convective parametrization scheme at ECMWF and their impact on the
636 mean and transient activity of the model in the tropics, ECMWF Research Department, Technical Memorandum
637 206, European Centre for Medium-range Weather Forecast, Reading, UK, 1994.
- 638 O’Gorman, P. A., Allan, R. P., Byrne, M. P. and Previdi, M.: Energetic Constraints on Precipitation Under Climate
639 Change, *Surv. Geophys.*, 33(3–4), 585–608, doi:10.1007/s10712-011-9159-6, 2012.
- 640 Pendergrass, A. G. and Hartmann, D. L.: Global-mean precipitation and black carbon in AR4 simulations,
641 *Geophys. Res. Lett.*, 39(1), 1–6, doi:10.1029/2011GL050067, 2012.
- 642 Pincus, R. and Stevens, B.: Paths to accuracy for radiation parameterizations in atmospheric models, *J. Adv.
643 Model. Earth Syst.*, 5(2), 225–233, doi:10.1002/jame.20027, 2013.
- 644 Ramanathan, V., Crutzen, P. J., Kiehl, J. T. and Rosenfeld, D.: Aerosols, Climate, and the Hydrological Cycle,
645 *Science* (80-.), 294(5549), 2119–2124, doi:10.1126/science.1064034, 2001.
- 646 Richardson, T. B., Forster, P. M., Andrews, T. and Parker, D. J.: Understanding the rapid precipitation response
647 to CO₂ and aerosol forcing on a regional scale, *J. Clim.*, 29(2), 583–594, doi:10.1175/JCLI-D-15-0174.1, 2016.
- 648 Richardson, T. B., Forster, P. M., Andrews, T., Boucher, O., Faluvegi, G., Fläschner, D., Hodnebrog, Ø., Kasoar,
649 M., Kirkevåg, A., Lamarque, J.-F., Myhre, G., Olivie, D., Samset, B. H., Shawki, D., Shindell, D., Takemura, T.
650 and Voulgarakis, A.: Drivers of Precipitation Change: An Energetic Understanding, *J. Clim.*, 31(23), 9641–9657,
651 doi:10.1175/JCLI-D-17-0240.1, 2018.
- 652 Roeckner, E., Stier, P., Feichter, J., Kloster, S., Esch, M. and Fischer-Bruns, I.: Impact of carbonaceous aerosol
653 emissions on regional climate change, *Clim. Dyn.*, 27(6), 553–571, doi:10.1007/s00382-006-0147-3, 2006.
- 654 Rotstayn, L. D. and Lohmann, U.: Tropical rainfall trends and the indirect aerosol effect, *J. Clim.*, 15(15), 2103–
655 2116, doi:10.1175/1520-0442(2002)015<2103:TRTATI>2.0.CO;2, 2002.
- 656 Samset, B. H., Myhre, G., Forster, P. M., Hodnebrog, Ø., Andrews, T., Faluvegi, G., Fläschner, D., Kasoar, M.,
657 Kharin, V., Kirkevåg, A., Lamarque, J. F., Olivie, D., Richardson, T., Shindell, D., Shine, K. P., Takemura, T.
658 and Voulgarakis, A.: Fast and slow precipitation responses to individual climate forcings: A PDRMIP multimodel
659 study, *Geophys. Res. Lett.*, 43(6), 2782–2791, doi:10.1002/2016GL068064, 2016.
- 660 Samset, B. H., Myhre, G., Forster, P. M., Hodnebrog, Ø., Andrews, T., Boucher, O., Faluvegi, G., Fläschner, D.,
661 Kasoar, M., Kharin, V., Kirkevåg, A., Lamarque, J.-F., Olivie, D., Richardson, T. B., Shindell, D., Takemura, T.
662 and Voulgarakis, A.: Weak hydrological sensitivity to temperature change over land, independent of climate
663 forcing, *npj Clim. Atmos. Sci.*, 1(1), 3, doi:10.1038/s41612-017-0005-5, 2017.
- 664 Shaw, T. A. and Voigt, A.: Tug of war on summertime circulation between radiative forcing and sea surface
665 warming, *Nat. Geosci.*, 8(7), 560–566, doi:10.1038/ngeo2449, 2015.
- 666 Stephens, G. L. and Hu, Y.: Are climate-related changes to the character of global-mean precipitation predictable?,
667 *Environ. Res. Lett.*, 5(2), doi:10.1088/1748-9326/5/2/025209, 2010.



- 668 Stevens, B., Giorgetta, M., Esch, M., Mauritsen, T., Crueger, T., Rast, S., Salzmann, M., Schmidt, H., Bader, J.,
669 Block, K., Brokopf, R., Fast, I., Kinne, S., Kornbluh, L., Lohmann, U., Pincus, R., Reichler, T. and Roeckner,
670 E.: Atmospheric component of the MPI-M Earth System Model: ECHAM6, *J. Adv. Model. Earth Syst.*, 5(2),
671 146–172, doi:10.1002/jame.20015, 2013.
- 672 Stier, P., Feichter, J., Kinne, S., Kloster, S., Vignati, E., Wilson, J., Ganzeveld, L., Tegen, I., Werner, M.,
673 Balkanski, Y., Schulz, M., Boucher, O., Minikin, A. and Petzold, A.: The aerosol-climate model ECHAM5-HAM,
674 *Atmos. Chem. Phys.*, 5(4), 1125–1156, doi:10.5194/acp-5-1125-2005, 2005.
- 675 Stier, P., Seinfeld, J. H., Kinne, S., Feichter, J. and Boucher, O.: Impact of nonabsorbing anthropogenic aerosols
676 on clear-sky atmospheric absorption, *J. Geophys. Res. Atmos.*, 111(18), 1–11, doi:10.1029/2006JD007147, 2006.
- 677 Stjern, C. W., Samset, B. H., Myhre, G., Forster, P. M., Hodnebrog, Ø., Andrews, T., Boucher, O., Faluvegi, G.,
678 Iversen, T., Kasoar, M., Kharin, V., Kirkevåg, A., Lamarque, J.-F., Olivie, D., Richardson, T., Shawki, D.,
679 Shindell, D., Smith, C. J., Takemura, T. and Voulgarakis, A.: Rapid Adjustments Cause Weak Surface
680 Temperature Response to Increased Black Carbon Concentrations, *J. Geophys. Res. Atmos.*, 122(21), 11,462–
681 11,481, doi:10.1002/2017JD027326, 2017.
- 682 Stjern, C. W., Richardson, T., Myhre, G., Faluvegi, G., Olivie, D., Stier, P., Samset, B. H., Fläschner, D.,
683 Takemura, T., Lamarque, J.-F., Smith, C. J., Forster, P., Kirkevåg, A., Boucher, O., Soden, B. J., Voulgarakis, A.,
684 Shindell, D., Kasoar, M., Hodnebrog, Ø., Kramer, R. J., Andrews, T. and Watson-Parris, D.: Quantifying the
685 Importance of Rapid Adjustments for Global Precipitation Changes, *Geophys. Res. Lett.*, 45(20), 11,399–11,405,
686 doi:10.1029/2018gl079474, 2018.
- 687 Suzuki, K. and Takemura, T.: Perturbations to Global Energy Budget Due to Absorbing and Scattering Aerosols,
688 *J. Geophys. Res. Atmos.*, 124(4), 2194–2209, doi:10.1029/2018JD029808, 2019.
- 689 Suzuki, K., Stephens, G. L. and Golaz, J.-C.: Significance of aerosol radiative effect in energy balance control on
690 global precipitation change, *Atmos. Sci. Lett.*, 18(10), 389–395, doi:10.1002/asl.780, 2017.
- 691 Tegen, I., Neubauer, D., Ferrachat, S., Drian, C. S. Le, Bey, I., Schutgens, N., Stier, P., Watson-Parris, D., Stanelle,
692 T., Schmidt, H., Rast, S., Kokkola, H., Schultz, M., Schroeder, S., Daskalakis, N., Barthel, S., Heinold, B. and
693 Lohmann, U.: The global aerosol-climate model echam6.3-ham2.3 -Part 1: Aerosol evaluation, *Geosci. Model
694 Dev.*, 12(4), 1643–1677, doi:10.5194/gmd-12-1643-2019, 2019.
- 695 Tiedtke, M.: A Comprehensive Mass Flux Scheme for Cumulus Parameterization in Large-Scale Models, *Mon.
696 Weather Rev.*, 117(8), 1779–1800, doi:10.1175/1520-0493(1989)117<1779:ACMFSF>2.0.CO;2, 1989.
- 697 Wang, C.: The sensitivity of tropical convective precipitation to the direct radiative forcings of black carbon
698 aerosols emitted from major regions, *Ann. Geophys.*, 27(10), 3705–3711, doi:10.5194/angeo-27-3705-2009,
699 2009.
- 700 Wang, H., Xie, S. P., Kosaka, Y., Liu, Q. and Du, Y.: Dynamics of Asian summer monsoon response to
701 anthropogenic aerosol forcing, *J. Clim.*, 32(3), 843–858, doi:10.1175/JCLI-D-18-0386.1, 2019.



- 702 Wang, Z., Lin, L., Yang, M., Xu, Y. and Li, J.: Disentangling fast and slow responses of the East Asian summer
703 monsoon to reflecting and absorbing aerosol forcings, *Atmos. Chem. Phys.*, 17(18), 11075–11088,
704 doi:10.5194/acp-17-11075-2017, 2017.
- 705 Zelinka, M. D., Myers, T. A., McCoy, D. T., Po-Chedley, S., Caldwell, P. M., Ceppi, P., Klein, S. A. and Taylor,
706 K. E.: Causes of Higher Climate Sensitivity in CMIP6 Models, *Geophys. Res. Lett.*, 47(1), 1–12,
707 doi:10.1029/2019GL085782, 2020.
- 708 Zhang, K., O'Donnell, D., Kazil, J., Stier, P., Kinne, S., Lohmann, U., Ferrachat, S., Croft, B., Quaas, J., Wan,
709 H., Rast, S. and Feichter, J.: The global aerosol-climate model ECHAM-HAM, version 2: sensitivity to
710 improvements in process representations, *Atmos. Chem. Phys.*, 12(19), 8911–8949, doi:10.5194/acp-12-8911-
711 2012, 2012.
- 712 Zhang, S.: On the Contribution of Fast and Slow Responses to Precipitation Changes Caused by Aerosol
713 Perturbations, Mendeley Data, V1, doi: 10.17632/8n2vj578r2.1, 2021
- 714 Zhang, S., Wang, M., J. Ghan, S., Ding, A., Wang, H., Zhang, K., Neubauer, D., Lohmann, U., Ferrachat, S.,
715 Takeamura, T., Gettelman, A., Morrison, H., Lee, Y., T. Shindell, D., G. Partridge, D., Stier, P., Kipling, Z. and
716 Fu, C.: On the characteristics of aerosol indirect effect based on dynamic regimes in global climate models, *Atmos.*
717 *Chem. Phys.*, 16(5), 2765–2783, doi:10.5194/acp-16-2765-2016, 2016.
- 718 Zhao, S. and Suzuki, K.: Differing Impacts of Black Carbon and Sulfate Aerosols on Global Precipitation and the
719 ITCZ Location via Atmosphere and Ocean Energy Perturbations, *J. Clim.*, 32(17), 5567–5582, doi:10.1175/jcli-
720 d-18-0616.1, 2019.
- 721 Zheng, B., Tong, D., Li, M., Liu, F., Hong, C., Geng, G., Li, H., Li, X., Peng, L., Qi, J., Yan, L., Zhang, Y., Zhao,
722 H., Zheng, Y., He, K. and Zhang, Q.: Trends in China's anthropogenic emissions since 2010 as the consequence
723 of clean air actions, *Atmos. Chem. Phys.*, 18(19), 14095–14111, doi:10.5194/acp-18-14095-2018, 2018.
- 724
725
726



727

728 **Table 1.** ECHAM6-HAM2 simulated multi-annual global averaged fast, slow, and total responses of atmospheric
729 energy budget terms (LP – the atmospheric latent heating rate from rainfall, ARC – atmospheric radiative cooling, SH
730 – sensible heat flux) and surface temperature (T) in response to increase of 10 times black carbon (BC) emission and 5
731 times sulphate (SUL) emission. ARC has been further decomposed into the contribution from aerosols, clouds and
732 clear-clean sky.

733

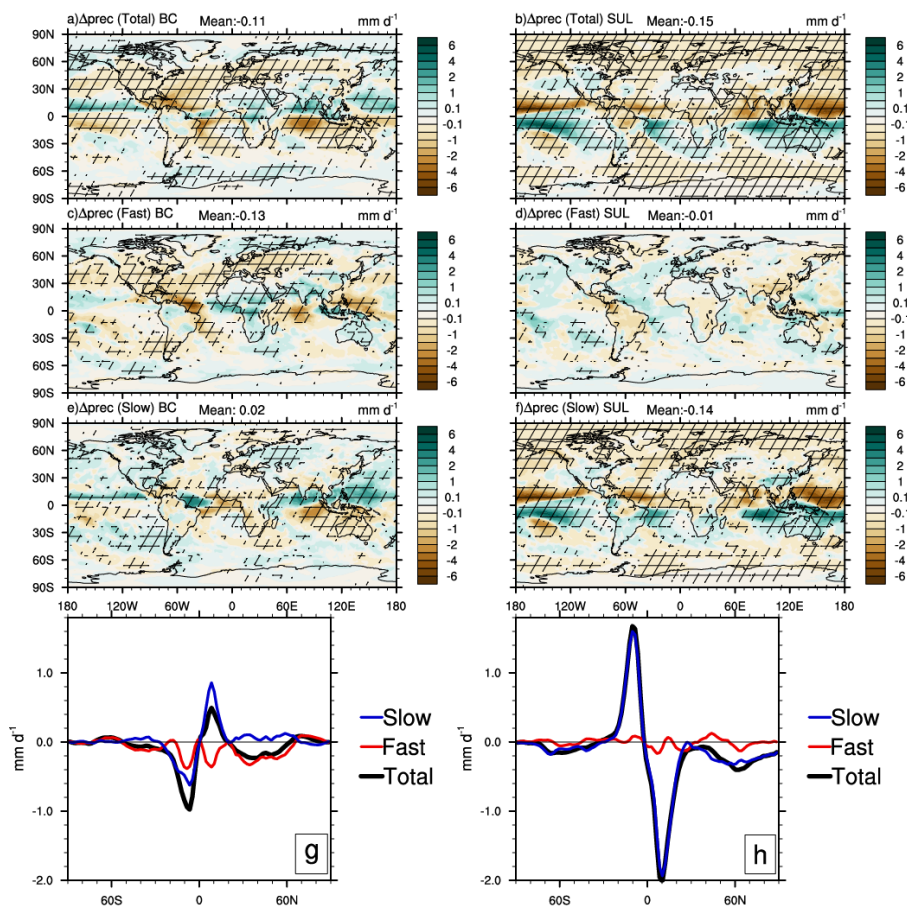
(W m ⁻²)	LΔP	ΔARC	ΔARC _{aerosol}	ΔARC _{cloud}	ΔARC _{cc}	-ΔSH	ΔT (K)
fast, 10BC	-3.64	-5.99	-8.42	0.93	1.50	2.41	-0.04
slow, 10BC	0.38	0.70	-0.41	-0.06	1.18	-0.35	0.47
total, 10BC	-3.26	-5.29	-8.83	0.87	2.68	2.06	0.43
fast, 5SUL	-0.20	-0.26	0.21	0.03	-0.50	0.06	-0.13
slow, 5SUL	-4.13	-3.82	-0.06	0.54	-4.30	-0.23	-1.75
total, 5SUL	-4.33	-4.08	0.15	0.57	-4.80	-0.17	-1.88

734

735

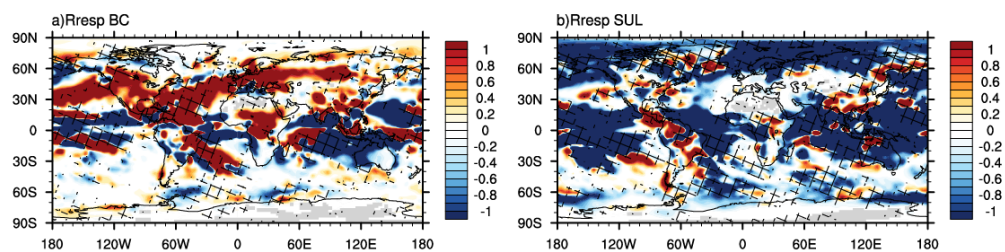
736

737



738
739 **Figure 1.** ECHAM6-HAM2 simulated geographical patterns of multi-annual mean precipitation change in response to
740 increasing (left column) 10 times BC emissions and (right column) 5 times SUL emissions for (first row) total, (second
741 row) fast, and (third row) slow responses. Hatching indicates where the changes are significant (90% confidence).
742 (fourth row) Zonal averages of changes in precipitation in terms of total, fast and slow responses to increasing (g) 10
743 times BC emission and (h) 5 times SUL emission.

744
745
746
747
748
749
750
751
752



753

754

755

756

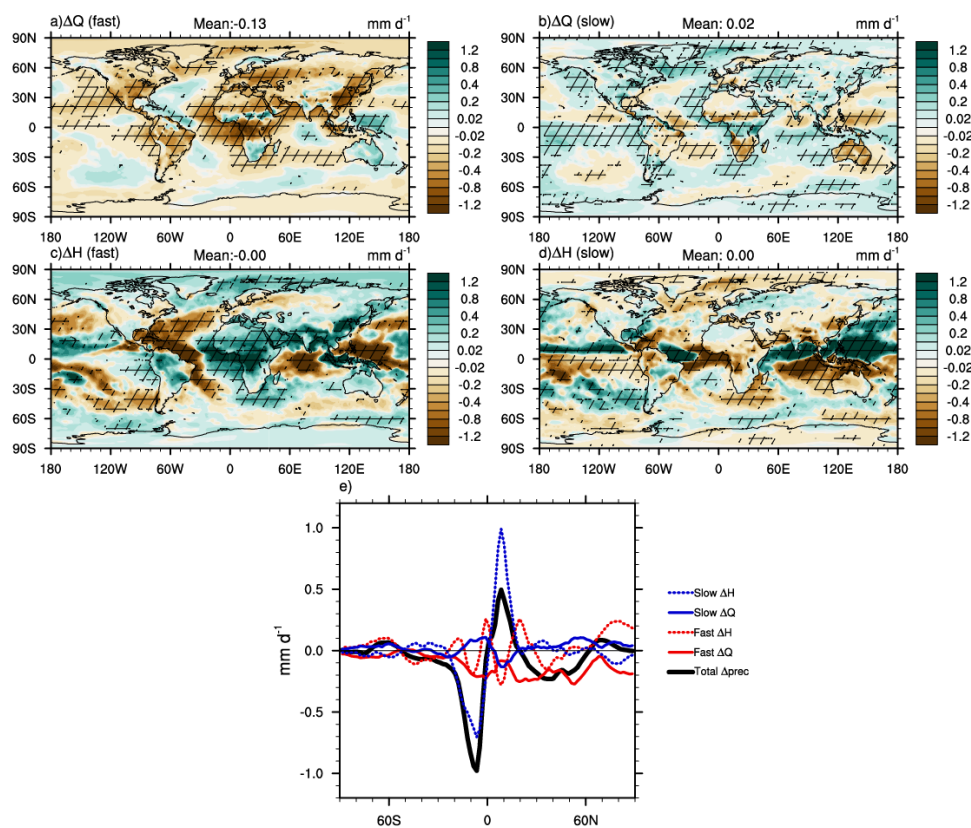
757

758

Figure 2. Response ratio of fast and slow responses (R_{resp}) (red denotes fast responses dominates the total responses and blue indicate slow responses dominates) of fast and slow responses for (a) BC cases and (b) SUL cases. Results have been normalised by total responses of precipitation. Hatching indicates the signs of fast and slow responses are same.



759
760



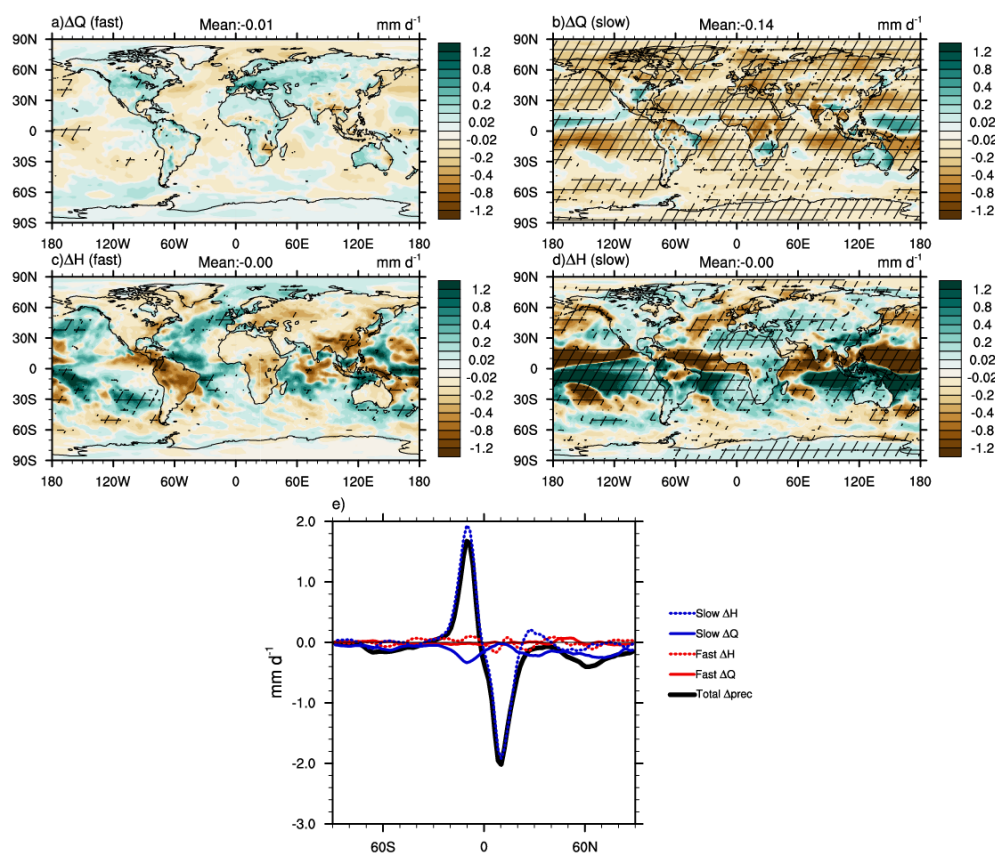
761

762 Figure 3. ECHAM6-HAM2 simulated geographical patterns of multi-annual mean changes in (first row) atmospheric
763 diabatic cooling (ΔQ) and (second row) dry static energy flux divergence (ΔH) for (left column) fast responses and
764 (right column) slow responses to 10 times BC emission. Hatching indicates where the changes are significant (90%
765 confidence interval through bootstrapping methods). (e) The zonal mean of total precipitation response and its
766 decompositions, including fast and slow responses of diabatic cooling and dry static energy flux divergence. All of them
767 are shown in equivalent precipitation units of mm d^{-1} .

768



769
770



771

772

773

774

775

776

777

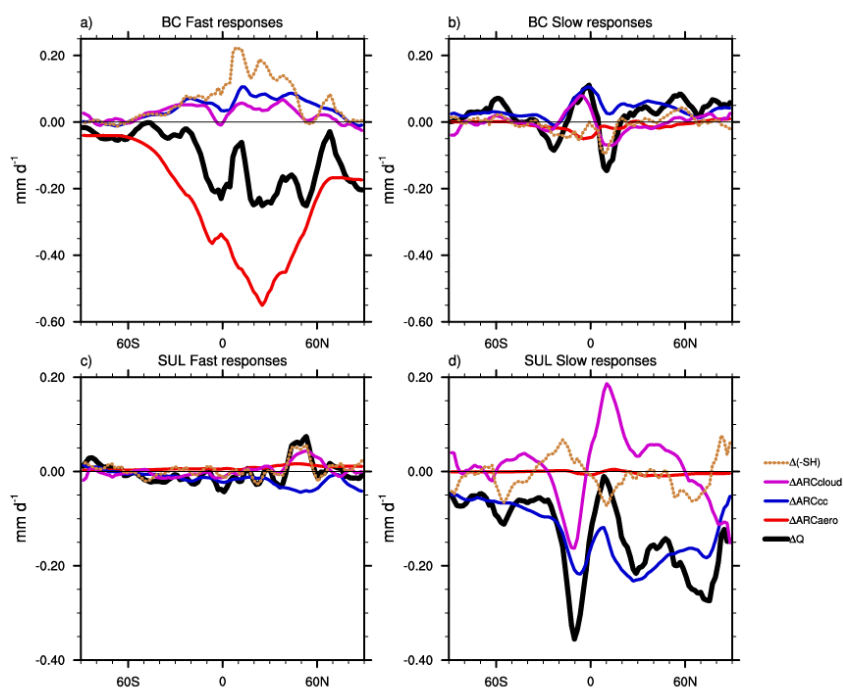
Figure 4. ECHAM6-HAM2 simulated geographical patterns of multi-annual mean changes in (first row) atmospheric diabatic cooling and (second row) dry static energy flux divergence for (left column) fast responses and (right column) slow responses to 5 times SUL emission. Hatching indicates where the changes are significant (90% confidence interval through bootstrapping methods). (e) The zonal mean of total precipitation response and its decompositions, including fast and slow responses of diabatic cooling and dry static energy flux divergence. All of them are shown in equivalent precipitation units of mm d^{-1} .

778

779



780



781

782 **Figure 5.** ECHAM6-HAM2 simulated multi-annual zonal mean of decomposed changes in atmospheric diabatic cooling
783 (ΔQ), including ARC changes from aerosols (ΔARC_{aero}), clouds (ΔARC_{cloud}), clear-clean sky ($\Delta\text{ARC}_{clear, clean}$),
784 downward sensible heat flux ($\Delta(-SH)$) for (a) fast responses in the BC case, (b) slow responses in the BC case, (c) fast
785 responses in the SUL case, and (d) slow responses in the SUL case. All items are shown in equivalent precipitation units
786 of mm d⁻¹.

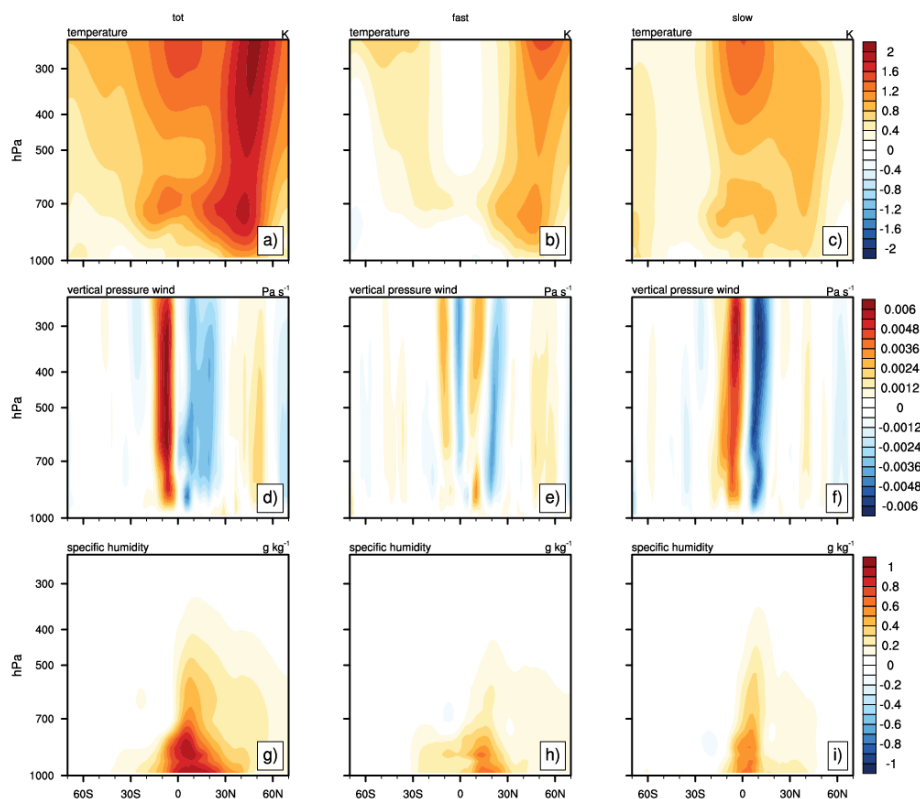
787

788

789



790
791



792

793

794

795

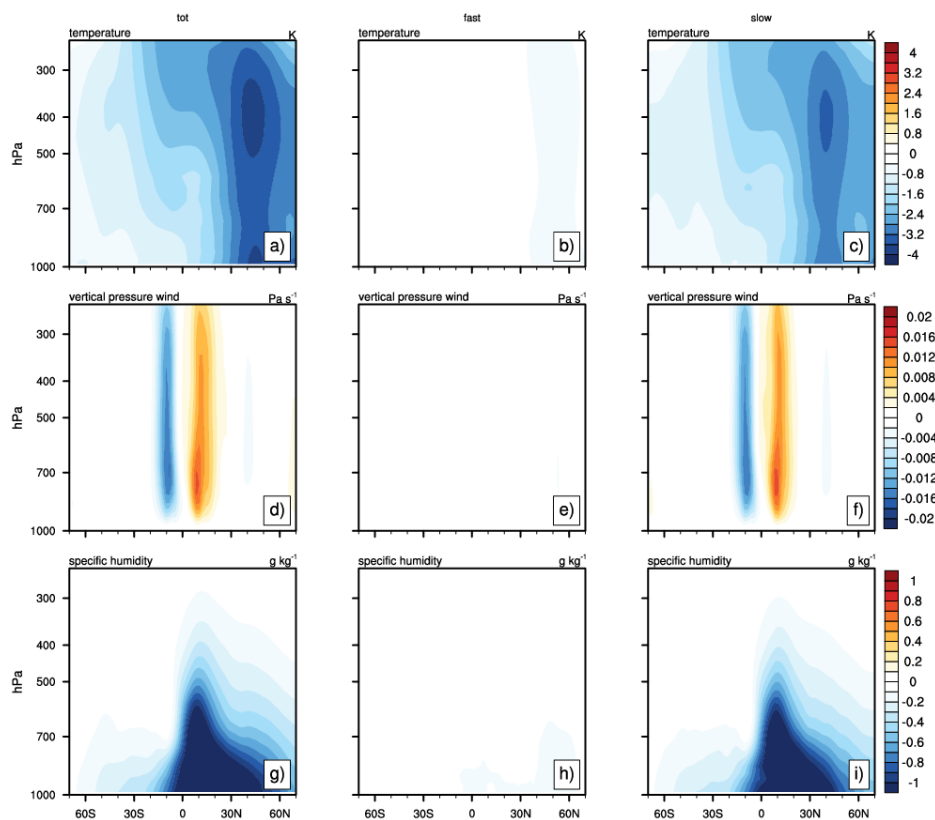
Figure 6. ECHAM6-HAM2 simulated multi-annual (left column) total, (middle column) fast, and (right column) slow responses of zonally averaged (a, b, c) temperature, (d, e, f) vertical pressure velocity, and (g, h, i) specific humidity in response to 10 times BC emission.

796

797



798
799
800



801
802

803 **Figure 7.** ECHAM6-HAM2 simulated multi-annual (left column) total, (middle column) fast, and (right column) slow
804 responses of zonally averaged (a, b, c) temperature, (d, e, f) vertical pressure velocity, and (g, h, i) specific humidity in
805 response to 5 times SUL emission.

806
807